International Journal of Mechanics and Energy (IJME)
Vol. 1, Issue 1, 2013, ISSN: 2286-5845

NUMERICAL INVESTIGATION OF FLOW OVER WIND TURBINE AIRFOIL NACA 23015

[1]Mohamed Mehdi Oueslati *, [1]Anouar Wajdi Dahmouni, [2]Mohieddine Ben Salah, [3]Faouzi Askri, [3]Sassi Ben Nasrallah

[1]*Laboratory of Wind Power Control and Energy Valorization of Waste (LMEEVED), Research and Technology Center of Energy Borj Cedria Technopark, B.P. 95, 2050 Hammam Lif, TUNISIA*

[2]*Laboratory of Thermal Process (LPT), Research and Technology Center of Energy, Borj Cedria Technopark, B.P. 95, 2050 Hammam Lif, TUNISIA*

[3]*Laboratory of Thermal and Energetic Systems Studies (LESTE), National Engineering School of Monastir (ENIM), Ibn Aljazzar Street, 5019 Monastir, TUNISIA*

Received December 14, 2012 / Accepted May 14, 2013

Abstract: To study the flow dynamic behavior of the NACA 23015 airfoil, used in many commercialized wind turbine, a computational fluid dynamic solving the streamfunction-vorticity formulation of Navier-Stokes equations using the Control Volume Method based on Finite Element (CVMFE) have been made to simulate the flow over the NACA 23015 at high angle of attack equal to 14° for Reynolds number equal to 1000. The Proper Orthogonal Decomposition (POD) method is adopted to analyze and extract the coherent motion structures in the flow behind the airfoil and the first two modes are used to determine the phase of the vortex shedding.

Key words: Streamfunction-vorticity formulation, Control volume based on finite element method, NACA 23015, POD analysis.

1. Introduction

The numerical simulation of unsteady flows around bluff bodies is an important topic in fluid mechanical investigation for a long time and affecting many industrial applications such as: vehicle design, flow around wings, wind turbine, aerodynamic building and several other applications.

An airfoil at a large angle of attack can be considered as a bluff body, and the flow structure behind it in general depends on the shear layer due to the separation of the boundary layer and the shear layer at the trailing edge which cause the presence of a relatively large backflow region and instabilities in the wake.

To more understand the wake behavior of the wind turbine airfoil NACA 23015 at high angle of attack equal to 14°and to analyze the temporal evolution of coherent structures, a numerical tool based on the stream-function-vorticity formulation of the Navier-Stokes equations for unsteady incompressible fluid flow using the control volume based on finite element method with an unstructured mesh have been developed and the proper orthogonal decomposition (POD) method introduced by [1] in the context of coherent structures based on the snapshot method have been used also.

In the literature various approaches are presented for the phase averaging method used to reconstruct the vortex evolution. Ref. [2] has used the pressure signal

*** Corresponding author:** Mohamed Mehdi Oueslati
E-mail: mehdi.oueslati@crten.rnrt.tn.

to trigger the sampling of the vortex shedding phases. Ref. [3] and [4] have proposed to use the first two principal modes obtained with the POD technique, in order to reconstruct the vortex evolution, whereas [5] have compared the phase averaged flow fields obtained with a trigger originated from the pressure signal with the POD-based approach. Ref. [5] found that an enhancement in the averaged velocity fields is obtained with the POD approach, since the phase angles is determined directly from the velocity fields to be averaged.

The control volume based on finite element method of [6] used in this work is a combination between the control volume method and the finite element method with conservation of the advantages of them both. Then, this method has been developed by many researchers such as [7], [8],…

The stream-function-vorticity formulation, is used here to calculate the flow characteristics, since it has several advantages in numerical simulations of steady and unsteady flows, such as the pressure term is eliminated from the governing equations, automatically satisfies the continuity constraint and it reduces the number of equations that must be resolved to simulate the flow.

2. Numerical Approaches

2.1 Governing Equation

The flow is assumed to be unsteady, incompressible, laminar and two-dimensional, and all the physical properties of the fluid are constant. The dimensionless governing equations, expressed in terms of vorticity and stream-function have written as following:

$$\frac{\partial \omega^*}{\partial t^*} + u^* \frac{\partial \omega^*}{\partial x^*} + v^* \frac{\partial \omega^*}{\partial y^*} = \frac{1}{\mathrm{Re}} \left(\frac{\partial^2 \omega^*}{\partial x^{*2}} + \frac{\partial^2 \omega^*}{\partial y^{*2}} \right) \quad (1)$$

$$\frac{\partial \omega^*}{\partial t^*} + div\left(\vec{U} \omega^* - \frac{1}{\mathrm{Re}} \overrightarrow{grad}(\omega^*) \right) = 0 \quad (2)$$

With ω^* the dimensionless vorticity, (u^*, v^*) the dimensionless velocity components, and Re is the Reynolds number. We note then $\omega^* = \omega$.

The Poisson's equation relating the stream-function and vorticity is shown as follows:

$$\frac{\partial^2 \psi}{\partial x^2} + \frac{\partial^2 \psi}{\partial y^2} = -\omega \quad (3)$$

With ψ is the stream function.

$$div(\overrightarrow{grad}(\psi)) = -\omega \quad (4)$$

2.1.1 Discretization of Vorticity Equation

We consider an element ΔV_N and a time interval Δt.

The integration of (2) is given by:

$$\underbrace{\int_t^{t+\Delta t} \underbrace{\iiint_V \frac{\partial \omega}{\partial t} dV}_{Accumulation\ Term} dt}_{} + \underbrace{\int_t^{t+\Delta t} \underbrace{\iiint_V div\left(\vec{j_\omega}\right) dV}_{Flux\ Term} dt}_{} = 0 \quad (5)$$

To discrtize the following equation we have used an implicit shame for the temporal term, a linear interpolation to determine the vorticity in each node, and the Simpson's rule for the numerical integration. The final equation obtained is given as follows:

$$\left(\omega_N - \omega_N^0\right) V_N + \Delta t \sum_{j=0}^{Ne-1} \left[A_{1j}^N \omega_N + A_{2j}^N \omega_{N_j} A_{3j}^N \omega_{N_{j+1}} \right] = 0 \quad (6)$$

then

$$\alpha_N^\omega \omega_N + \sum_{j=0}^{Ne-1} \gamma_{N_j}^\omega \omega_{N_j} = \beta_N^\omega \quad (7)$$

2.1.2 Discretization of Poisson Equation

The integration of the Poisson equation for the stream function given in (4) is written as follow:

$$\underbrace{\iiint_{V_C} div(\overrightarrow{grad}(\psi)) dV_C}_{Q_4} = \underbrace{\iiint_{V_C} -\omega dV_C}_{Q_5} \quad (8)$$

With the same manner, as described below, the final equation obtained after discretization is given by:

$$\sum_{j=0}^{Ne-1} \left[C_{1,j}^N . \psi_N + C_{2,j}^N . \psi_{N_j} + C_{3,j}^N . \psi_{N_{j+1}} \right] = -\Delta V_N \omega_N \quad (9)$$

2.2 Boundary Condition

To solve this problem many investigations are made. Ref. [9], [10], and [11], note that the convective boundary condition is most suitable: it makes possible

to reduce the length of the field to be studied and to model the flow without the appearance of re-circulation zones at the outflow. The convective boundary condition is written as follow:

$$\begin{cases} \dfrac{\partial u}{\partial t} + u_{avr}\dfrac{\partial u}{\partial x} = 0 \\ \dfrac{\partial v}{\partial t} + u_{avr}\dfrac{\partial v}{\partial x} = 0 \end{cases} \tag{10}$$

with u_{avr} is the average velocity.

That gives in streamfunction formulation:

$$\begin{cases} \dfrac{\partial}{\partial t}\left(-\dfrac{\partial \psi}{\partial y}\right) + u_{avr}\dfrac{\partial}{\partial x}\left(-\dfrac{\partial \psi}{\partial y}\right) = 0 \\ \dfrac{\partial}{\partial t}\left(\dfrac{\partial \psi}{\partial x}\right) + u_{avr}\dfrac{\partial^2 \psi}{\partial x^2} = 0 \end{cases} \tag{11}$$

Then we obtain that:

$$\frac{\partial}{\partial t}\left(-\frac{\partial \psi}{\partial y}\right) = u_{avr}\left(\frac{\partial^2 \psi}{\partial x^2} - \omega\right) \tag{12}$$

2.3 Unstructured Mesh

In our work, an unstructured mesh generator is used, which is developed by the co-authors. The mesh generator is based on the Delaunay-Voronoï method which allows us to model and discretize objects with complex geometries.

The spatial domain is subdivided into three-node triangular elements. As shown in Fig. 1, the control volume is created around each node N by enjoining the centroids G_j of the elements to midpoints M_1 and M_2 of the corresponding sides. Each element has two faces, M_1G_j and G_jM_2; bounding the sub-control volume around N; and each control volume is constructed by adding all sub-volumes $NM_1G_jM_2N$. The mesh elements are constructed one by one, from the contour data of the considered domain.

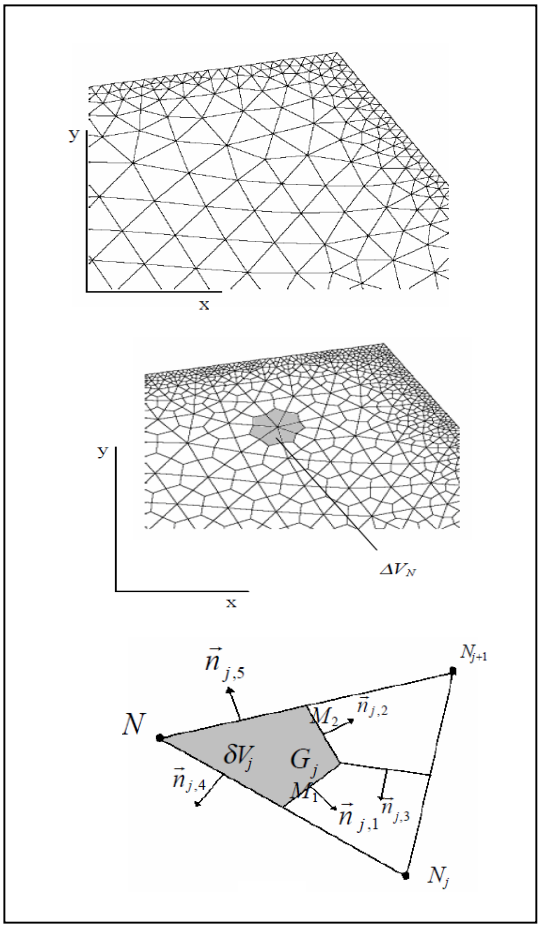

Fig. 1 Mesh construction

2.4 Proper Orthogonal Decomposition

The basic idea of the proper orthogonal decomposition (POD), is the determination of a set of orthogonal functions or eigenmodes, with random coefficients that represent the field as good as possible based on an energy-weighted measure. The eigenmodes are stored in descending order with respect to their energy content with the dominant eigenmodes representing the characteristic features of the flow.

The implementation of the POD is based on the method of snapshots [12], providing a decomposition of the velocity field $f(x)$:

$$f_n(x) = \sum_{n=1}^{N} a_n \psi_n(x) \tag{13}$$

with $f_n(x) = f(x, nt)$ is an instantaneous flow field or snapshots and N the total number of snapshots. Since the eigenmodes $\psi_n(x)$ are orthonormal, the respective mode coefficients a_n are uncorrelated:

$$\langle a_n a_m \rangle = \lambda_n \delta_{nm} \quad (14)$$

Here the operator $\langle \ldots \rangle$ denotes ensemble averaging. The eigenvalue λ_n represents the contribution of the corresponding eigenmodes $\psi_n(x)$ to the total energy of the field. According to [12], the eigenmodes have the form

$$\psi(x) = \sum_{n=1}^{N} \zeta_n f_n(x) \quad (15)$$

Where the coefficients ζ_n are determined by the eigenfunctions of the spatial correlation matrix C given by the inner product of the velocity fields at times n and m:

$$C_{nm} = \frac{1}{N}(f_n, f_m) \quad (16)$$

Note that POD defines a mathematical framework and the association of the eigenfunctyions of the correlation operator with coherent structures is based on interpretation and fluid dynamical intuition.

3. Results and Discussions

3.1 Validation Case: Flow Over Square Cylinder

Computations have been carried out for the flow around a square cylinder with diameter D, inside the horizontal channel. The square cylinder is symmetrically placed in the channel axis as indicated in Fig. 2. In order to reduce the influence of inflow and outflow boundary conditions, the length of the channel was set $\frac{L}{D} = 50$ and an inflow length of $l = \frac{L}{4}$.

The computations were performed using 12*167 and 17*229. In the region near the square cylinder the mesh is finner than in the region near the outlet of the channel (Fig.2).

To validate our numerical code we have compared the velocity components u profile of the flow around the square cylinder with $\frac{1}{8}$ blockage ratio and a Reynolds number equal to 100, with the numerical work of Bernsdorf [13] using the Lattice Boltzmann Method (LBM) .

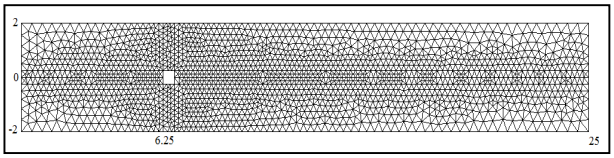

Fig. 2 Unstructured mesh around square cylinder

We obtain the following profiles of velocity components:

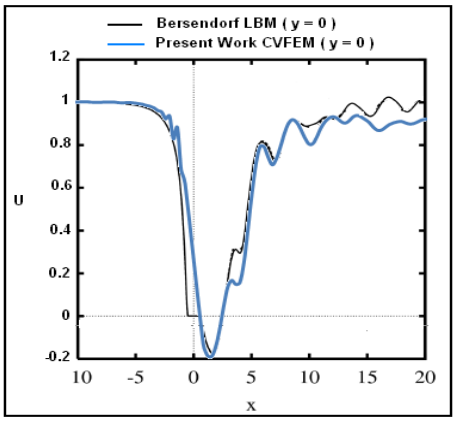

Fig. 3 Comparaison between LBM of Bernsdorf and the present work with CVFEM along the centerline y = 0 at Re = 100.

In Figure 3 we can observe that our results are in good agreement with those of [13], especially in the length of the zone of re-circulation, then a light difference between the two curves is observed at the outlet, due to the difference between the properties of the fluid and the numerical method used.

3.2 Flow Topology over NACA 23015

To study the flow past the wind turbine airfoil NACA 23015, the airfoil is embedded in a rectangular channel has width equal to 2 and a length equal to 8. The flow in the inlet is assumed uniform flow and the airfoil is located near the inflow.

In many research works, the NACA 23015 attain its maximum lift coefficient at an angle of attack equal to 14°, for that we will choose this angle of attack in this work and et Reynolds number equal to 1000.

In order to verify that the results are grid independent, three unstructured mesh are used forming by 1576 nodes, 2003 nodes, and 2543 nodes respectively, and refined near the leading edge and the trailing edge of the airfoil.

The figure 5 shows the velocity component *u* profile for the different cases. The results show that the velocity profiles are very close especially in the cases of 2003 nodes and 2543 nodes and the maximum difference is less than 3%. For that we have chosen to work with the unstructured mesh which is composed of 4890 triangles and 2543 nodes.

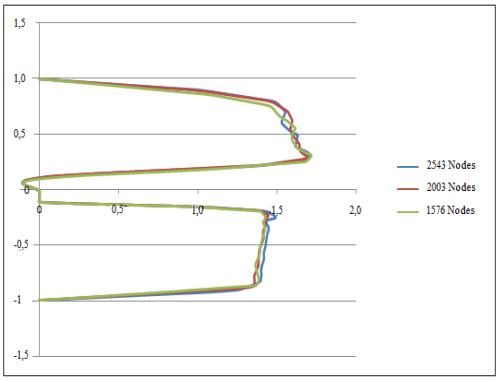

Fig.4 Velocity component u profile for different mesh

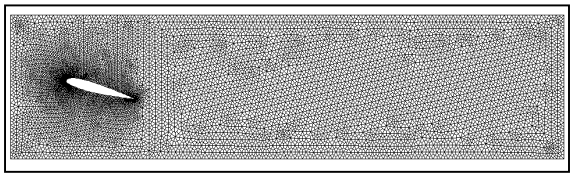

Fig. 5 Unstructured mesh around the airfoil NACA 23015

The results of simulation show an interesting mechanism of a detachment of vortex over the airfoil which we will describe it below:

As the flow evolves with time, the Fig.6-a- shows, a separation bubble, (b), which builds up almost in the medium of the upper surface of the airfoil, and the starting vortex, (a) , originating from moving the rear stagnation point to the trailing edge, is convected out in the wake flow. As the separation bubble, (b), grows bigger and move further downstream, two new separation bubbles (c) and (d), are formed respectively near the medium of the upper surface and at the leading edge as seen in Fig. 6-b- .

In between the primary separation bubble, (b), and the newly created separation bubble, (d), a counter clockwise rotating bubble, (c), exists. The structures formed by (b), (c), and (d) is felt as a thickening of the airfoil and the flow is attached at the trailing edge. The counter rotating bubble, (c), and the primary bubble, (b), are enlarged as seen in Fig.6-c- .

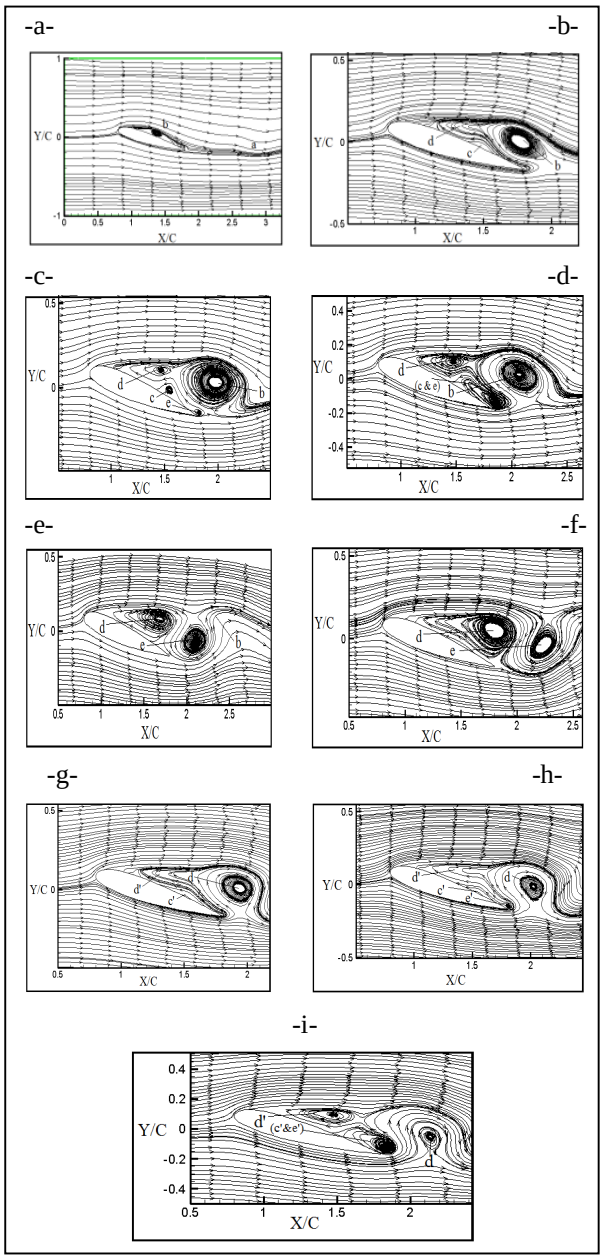

Fig. 6 Streamlines of NACA 23015 for different time steps

As the primary bubble, (b), is further enlarged the flow de-attaches at the trailing edge and a new counter rotating trailing edge vortex, (e), is formed.

In Figure 6-d-, the trailing edge vortex, (e), has become bigger and the vortex pair consisting of (c) and (e) begins to merge. This merging process together with a convection and diffusion process governs the movement of a primary vortex, (b), into the wake. In Figure 6-e-, at the trailing edge a large separation area exists, (e), and at the leading edge the vortex, (d), has been elongated.

The Figure 6 -f- indicates that the vortex, (d), is more elongated and occupies the upper surface from the separation point to the trailing edge and the trailing edge vortex, (e), is convected in the wake.

In function of the time (Fig.6-g-) the vortex, (d), lives the airfoil to the wake and two new vortex are generated, (c') and (d'), located respectively near the middle of the upper surface and the leading edge. In Figure 6-h- a forth vortex, (e'), is created at the trailing edge of the airfoil, and it will grow with time to merge with the vortex, (c').

The vortex, (d'), is elongated and the vortex, (d), lives completely the airfoil and convected in the wake, as shown in Fig.6-i- in which the same phenomena of the Fig.6-d- is repeated.

In other hand, to characterize the flow behind the airfoil the streamlines, the velocities components U and V, and the vorticity has been presented as shown in Fig. 7, 8, 9, and 10 respectively.

Those Figures show the formation and detachment of the vortex from the lower shear layer. The wake shear layer interacts with each other by drawing fluid, thus forming alternating vortex shedding downstream. This is similar to the Karman vortex street from a circular cylinder.

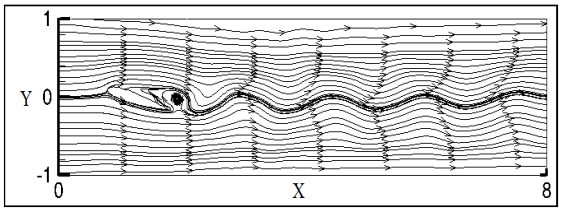

Fig. 7 Streamlines over the NACA 23015

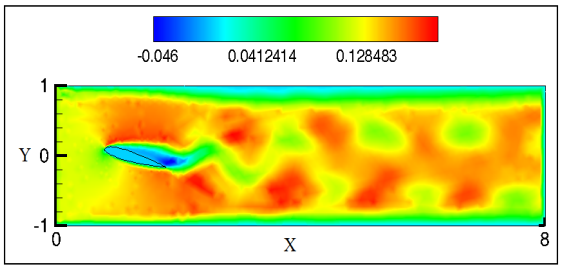

Fig.8 Velocity component U/Ue, for Re = 1000 and 14° angle of attack

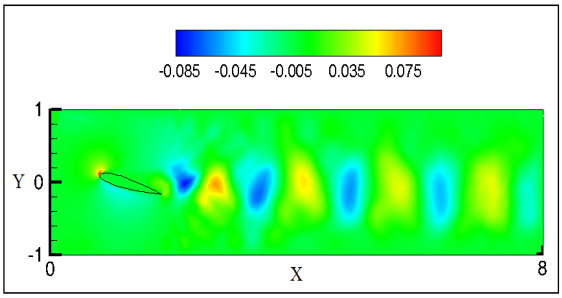

Fig. 9 Vertical velocity component V/Ue, for Re = 1000 and 14° angle of attack

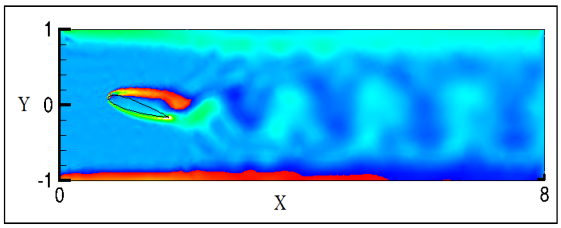

Fig. 10 Vorticity field over the NACA 23015 for Re=1000 and 14° angle of attack.

3.3 POD Analysis

Proper orthogonal decomposition (POD) is applied in order to identify and characterize coherent structures in the wake flow. The implementation of the POD is based on the method of snapshots and the ensemble of 200 snapshots associated with time difference equal to $\Delta t = 0.5$ is analyzed.

Moreover, only the vertical components are used which seem to be more pertinent to the identification of coherent structures in the airfoil's wake, since the boundaries of the coherent patterns are smeared.

The POD analysis yields a number of eigenmodes and eigenvalues equal to the number of snapshots included. The eigenmodes are sorted in descending order with respect to their relative contribution to the total energy of the fluctuating vertical motion, given by the respective eigenvalues.

The percentage of the total energy of the fluctuating motion contained by each mode for the numerical simulation at Re = 1000 based on the chord length of the airfoil is presented in Fig. 11.

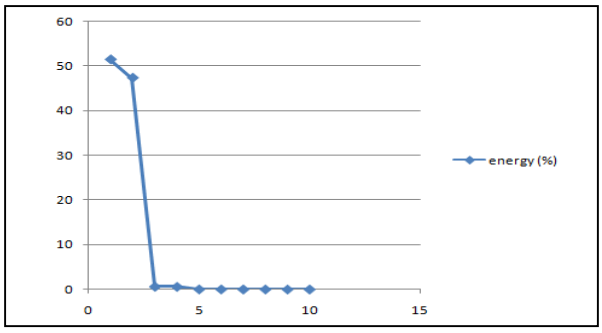

Fig. 11 Energy mode

The first issue observation is the importance energy of the two first modes. Together they contain more than 97% of the total energy of the fluctuating vertical motion in the wake. Then the successive energy content of the successive eigenmodes rapidly drops.

The first four normalized POD eigenmodes for Re = 1000 are depicted in Fig. 12. The first two modes present a similar pattern, consisting of a successive of large-scale spatial structures with alternating sign, which is consistent with the acknowledgement of them being a mode pair. The effect of superimposing both modes is to introduce the convection of the flow pattern they present.

3.4 Phase Averaged Using POD Coefficients

The observations made in the previous paragraph suggest that the dynamics of dominant periodic vortex shedding can be described by a low order flow model, i.e. a reconstruction of the flow field incorporating only the first two POD modes:

$$w'_{LOM}(x) = a_1\psi_1(x) + a_2\psi_2(x) \qquad (17)$$

The subscript LOM denotes low order model and (a_1, a_2) are the mode coefficients associated with the first two modes, determined from the projection on the POD modes. Since the modes are an orthonormal set, the coefficients a_i are normalized by $\sqrt{2\lambda_i}$

Furthermore the vortex shedding phase angle φ is a linear function of time, corresponding to $\varphi = 2\pi f_0 t$, and the evolution of the mode coefficients is given by:

$$a_1(\varphi) = \sqrt{2\lambda_1}\cos(\varphi) \qquad (18)$$

$$a_2(\varphi) = \sqrt{2\lambda_2}\sin(\varphi) \qquad (19)$$

Figure 13 (left) represent the periodic variation of the distribution of the mode coefficient a_1 and a_2 in function of the mode number.

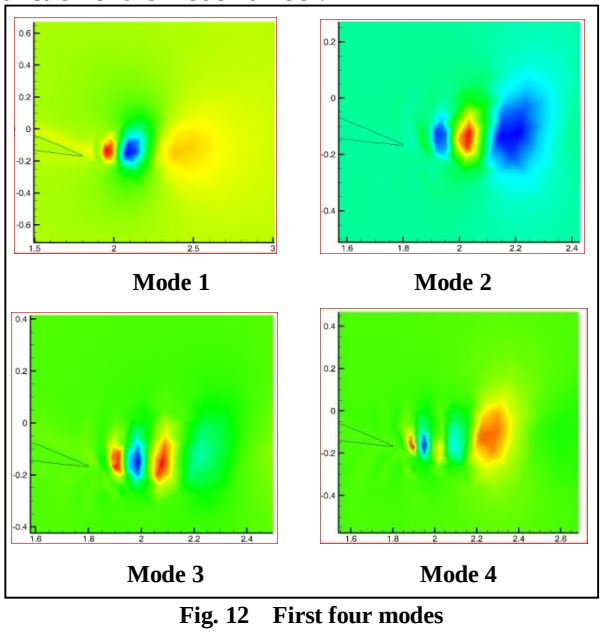

Fig. 12 First four modes

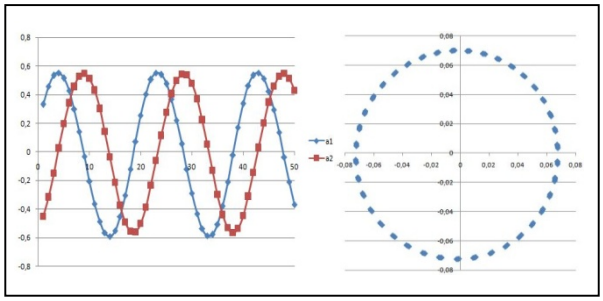

Fig. 13 a_1 and a_2 distributions

The figure 13 (right) illustrate the distribution of points in the normalized coefficient plane $\left(\frac{a_1}{\sqrt{2\lambda_1}}, \frac{a_2}{\sqrt{2\lambda_2}}\right)$, describing a circle as the same results described by [3] in the case of coherent motion in absence of higher order harmonics as well as random turbulent fluctuations.

The reconstruction of the vorticity contours at different phase angles of shedding vortex -45°, 0.63°, 47°, and 85° are presented in fig. 14.

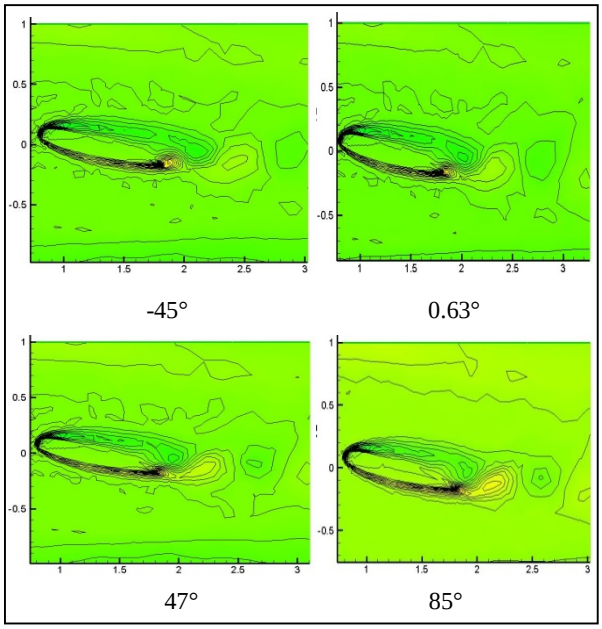

Fig. 14 Vorticity contours in different phase angles

4. Conclusion

A numerical code based on stream function-vorticity formulation of Navier Stokes equations have been elaborated and validated in the case of flow over square cylinder using the control volume based on finite element method.

The process of the detachment of the flow over the NACA 23015 have been described and analyzed at 14° angle of attack and Reynolds number equal to 1000. The different physics parameter: streamlines, velocity component, and vorticity have been plotted.

The Proper Orthogonal Decomposition (POD) is used to study the topology of the flow. The dynamics of the dominant periodic vortex shedding have been described by a low order flow model and the phase of shedding vortex is determined.

References

[1] J. L. Lumely, The structure of inhomogeneous turbulent flows. In Atmospheric Turbulence and Radio Wave Propagation, ed A. M. Yaglom, V. I. Tatarski, Nakua, Moscow, (1967) 166-178.

[2] M . Braza, R. Perrin, Y. Hoarau, Turbulence properties in the cylinder wake at high Reynolds numbers, J. Fluids Struct. 22 (2006) 757-771.

[3] M. Ben Chiekh, M. Michard, N. Grosjean, J. Bèra, Reconstruction temporelle d'un champ aérodynamique instationnaire à partir de mesures PIV non résolues dans le temps, [Proc 9e Conf. Francophone de Vélocimétrie Laser. Bruxelles, p. D.8.1-8, 2004].

[4] K. Mulleners, A. Henning, M. Raffel, Investigations of trailing edge stall on 2d airfoil, [14th Symp. On applications of laser techniques to fluid mechanics. Portugal, p. 1-11, 2008].

[5] R. Perrin, M. Braza, E. Cid, S. Cazin, A. Barthet, A. Sevrain, A. Mockett, F. Thiele, Phase-averaged measurements of the turbulence properties in the near wake of a circular cylinder at high Reynolds number by 2C-PIV and 3C-PIV, Exp Fluids. , 42 (2007) 93-109.

[6] H. J. Saabas, B. H. Baliga, Co-located equal-order control volume finite element method for multidimensional incompressible fluid flow part I: Formulation, Numer. Heat Tr. b-fund., 26 (1994) 409-424.

[7] G. E. Schneider, M. J. Raw, A Skewed Positive Influence Coefficient Upwinding Procedure for Control Volume

Based Finite Element Convection Diffusion Computation, Numer. Heat Transfer, 11 (1987), 363-390.

[8] C. Prakash, S. V. Patanker, A Control Volume Based Finite Element Method for solving the Navier-Stokes Equations Using Equal Order Velocity Pressure Interpolation, Numer. Heat Transfer, 8 (1985) 259-280.

[9] H. Abbassi, Etude par la méthode des volumes finis à base d'éléments finis de l'écoulement et du transfert de chaleur dans un canal plan contenant un obstacle, PhD. Thesis, University science of Tunis , Tunisia, (2001).

[10] M. A. Ol'shanskii, V. M. Staroverovon, simulation of outflow boundary conditions in finite difference calculations for incompressible fluid, Int. J. Num. Meth. Fl., (2000) 499-534.

[11] G. Comini, M. Manzan, G. Cortella, Open boundary conditions for the steamfunction-Vorticity formulation of unsteady laminar convection, Numer. Heat Tr. b-fund, 31 (1997) 217-234.

[12] L. Sirovich, Turbulence and the dynamics of coherent structures; part I – III, Quart. Of Appl. Math., 45 (1987) 561.

[13] J. M. Bernsdorf, Simulation of complex flow and Multi-Physics with Lattice-Boltzmann Method, PhD. Thesis, University Amesterdam, Holland, (2008).